# Journal of Materials Chemistry A

Accepted Manuscript


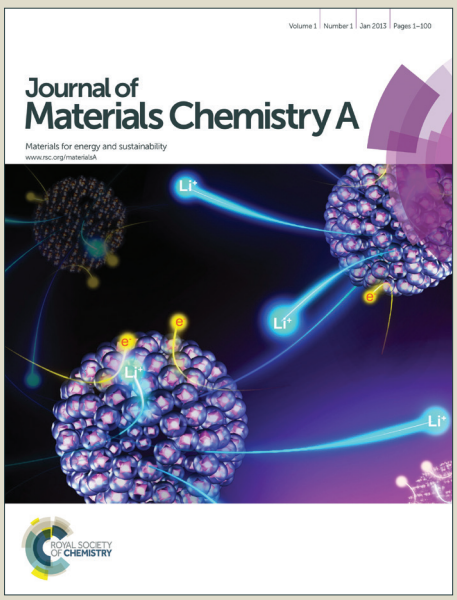





ROYAL SOCIETY OF CHEMISTRY

www.rsc.org/materialsA

# Novel heterostructures by stacking layered molybdenum disulfides and nitrides for solar energy conversion

*Hui Zhang*[a], *Yan-Ning Zhang*[a,b], *Hao Liu*[b], *Li-Min Liu*[a*]

[a]*Beijing Computational Science Research Center, Beijing 100084, China.*

[b]*Chengdu Green Energy and Green Manufacturing Technology R&D Center, Chengdu, Sichuan, 610207, China*

Email: limin.liu@csrc.ac.cn

**Abstract**

Two-dimensional graphene-like materials have attracted great attentions for the further development of nanoscale devices. In this work, the structural, electronic and optical properties of free-standing graphene-like nitrides XN (X=B, Al and Ga) are studied by density functional calculations with the inclusion of the nonlocal van der Waals correction. The results show that all the studied nitrides are thermodynamically stable and their electronic structures can be easily tuned by forming the heterostructure with $MoS_2$ monolayer. Although GaN and AlN monolayers remain the indirect band gap of bulk, $MoS_2$-AlN and $MoS_2$-GaN heterostructures have suitable direct gaps, complete electronic-hole separation and fascinating visible light adsorption, promising for solar energy applications. Additionally, the $MoS_2$-AlN heterostructure is a good candidate for enhanced photocatalytic activity of hydrogen generation from water.

Keywords: nitrides, $MoS_2$, heterostructures, photocatalysis

## 1. Introduction

The discovery of graphene has intrigued tremendous studies on novel low-dimensional materials[1-4] over the past few years due to its unique electronic structure and high charge carrier mobility[5]. Nevertheless, the absence of intrinsic band gap hampers the direct applications of graphene in widespread devices, such as field effect transistor (FET) and photocatalysis.[6] Consequently exploring new graphene-like 2D materials that exhibit unique and fascinating physical properties compared with their bulk counterparts is one of the most active fields to address this challenge.[7] Abundant accomplishments make 2D materials prosperous beyond carbon-based materials including elements and compounds[8-11].

There are two typical routes to fabricate 2D materials: one is to exfoliate free-standing stable low-dimensional materials from van der Waals solids, the other is to fabricate 2D heterostructures from the covalent bonding materials[12]. Taking the zinc-blende ZnSe as an example, the formation of large-area freestanding ZnSe monolayer triggered a way to get 2D heterostructures from non-layered compounds[13]. Moreover, the manipulation of electronic structures in heterostructures, by changing different materials and layer thickness, has been widely explored so as to meet distinct application requirements.[14] Many promising features, such as tunable band gaps and visible light response, have been reported for graphene nanocomposites and its analogues, such as *h*-BN, $C_3N_4$, and $MoS_2$.[15-17] The advantages of 2D heterostructures offer great potentials as functional materials with high performances. For example, $MoS_2$-$TiO_2$ heterostructures[18] show enhanced photocatalytic efficiency and give the hydrogen production rate of 1.6 mmol $h^{-1}g^{-1}$. Vertically stacked graphen-$MoS_2$-metal heterostructures are fabricated as a new generation field-effect-transistors[19] with high on-off ratio $>10^3$ and current density of up to 5000 A $cm^{-2}$.

The III–V compounds, especially nitrides XN (X=B, Al and Ga) with hexagonal wurtzite or cubic zinc-blende structures, are basic semiconductors for optoelectronics. Monolayer graphene-like BN, denoted as *g*-BN, has been fabricated experimentally[20], but is not a good photocatalyst due to the large band gap (~6.07 eV)[21, 22]. Thus, it is naturel to wonder whether the other graphene-like monolayer nitrides, such as *g*-AlN and *g*-GaN, can be thermodynamically stable and also have extraordinary physical properties. On the other hand, the previous works have revealed that layered transition metal dichalcogenides (TMD) exhibit versatile electronic structures.[23-26] For example, monolayer $MoS_2$ transforms to direct semiconductor of ~2.0 eV from indirect bulk one, which is important for the applications in photocatalysis and FET.[27, 28] Therefore, we may expect some excellent properties in $MoS_2$-XN heterostructures if they are stable.

The purpose of this study is to unveil a new group of graphene-like single-layer 2D materials *g*-XN (X=B, Al and Ga). Particular attention will be focused on the following questions: (i) Is it feasible to synthesize these single-layer materials? (ii) What are the electronic properties of these monolayers? (iii) What fantastic properties can heterostructures possess by combing graphene-like *g*-XN (X=B, Al and Ga) with

other single-layer materials, such as $MoS_2$? The calculated results exhibit the good stabilities of the free-standing 2D graphene-like AlN and GaN monolayers beyond BN. The proposed $MoS_2$-AlN and $MoS_2$-AlN heterostructures possess many novel properties, such as moderate band gap, suitable band edge positions, electronic-hole separation, and fascinating visible light adsorption, which enable them great potential applications for solar energy conversion and photocatalysis. Our extensive investigation extends the scope of 2D structures and brings out novel properties for solar energy conversion applications.

## 2. Methodology

In this work, all density functional theory (DFT) calculations were performed with Vienna Ab Initio Simulation Package (VASP)[29, 30]. Projector-augmented-wave (PAW) potentials[31] were used to account electron-ion interactions. The generalized gradient approximation (GGA) with the Perdew-Burke-Ernzerhof (PBE) functional[32] was used to treat the electron exchange correlation interactions. The more accurate the Heyd-Scuseria-Ernzerhof (HSE06) hybrid functional is used to determine the band gaps and optical properties. The vdW interaction is corrected by the DFT-D2 approach[33].

To remove spurious interactions between neighboring structures due to periodic calculations, a vacuum layer thickness larger than 10 Å was employed between the slabs. We used the energy cutoff of 600 eV, and a (16×16×1) Monkhorst-Pack *k*-point grid to sample the 2D Brillouin zone (BZ)[34]. The equilibrium geometries were fully optimized with both the lattice vectors and atom coordinates relaxed with the tolerance of less than 0.01eV/Å on each atom. The phonon calculations were performed by using the direct approach implemented in Phonopy package[35]. The Real-space force constants were calculated from the Hellmann-Feynman forces by introducing displacements to supercells based on finite displacement method[36]. Then the dynamical matrices, phonon frequencies were obtained via the force constants.

## 3. Results and discussion

### 3.1 *g*-XN (X=B, Al and Ga) monolayers

The atomic configurations of *g*-XN monolayers are shown in **Fig. 1(a)**. The *g*-XN monolayer has a 2D honeycomb hexagonal lattice with two atoms in the unit cell, X atom at (0, 0, 0) and N atom at (1/3, 2/3, 0). When X = B, Al and Ga, the optimized lattice constants *a* of *g*-XN are 2.51 Å, 3.15 Å, and 3.26 Å, and the bond length of XN are 1.45 Å, 1.81 Å, and 1.88 Å, respectively.

The phonon dispersion spectrum is a reliable tool to check if the virtue structure is stable.[37] A stable structure has all positive phonon frequencies for all modes over the Brillouin zone, while imaginary frequencies appears when the structure is dynamically unstable. In phonon calculations, 6×6 supercells were employed and the first BZ was sampled by 4×4 K-meshes. The full phonon dispersion spectra for the three monolayers along the high-symmetry directions in Brillouin zone are shown in **Fig. 1(b)**. No any imaginary vibration frequency appears for each structure, implying

that they have high phonon stability. As the *g*-BN monolayer has been successfully fabricated by experiments[8], we may expect the fabrication of the other two monolayers in the future. The electronic band structures shown in **Fig. 1(c)** suggest that monolayer *g*-BN, AlN and GaN are all indirect band gaps. The monolayer *g*-BN has a large band gap of 4.69 eV in good agreement with previous GGA value of 4.56 e,[38] but is underestimated than experimental 6.07 eV as usual[21]. In contrast, *g*-AlN exhibits a decreased band gap of 2.75 eV, and *g*-GaN has the smallest band gap of 2.00 eV. Compared with the bulk nitrides, the band gaps of 2D monolayers are decreased, e.g. by 33% for AlN (4.1 eV for wurtzite structure with GGA-PBE).

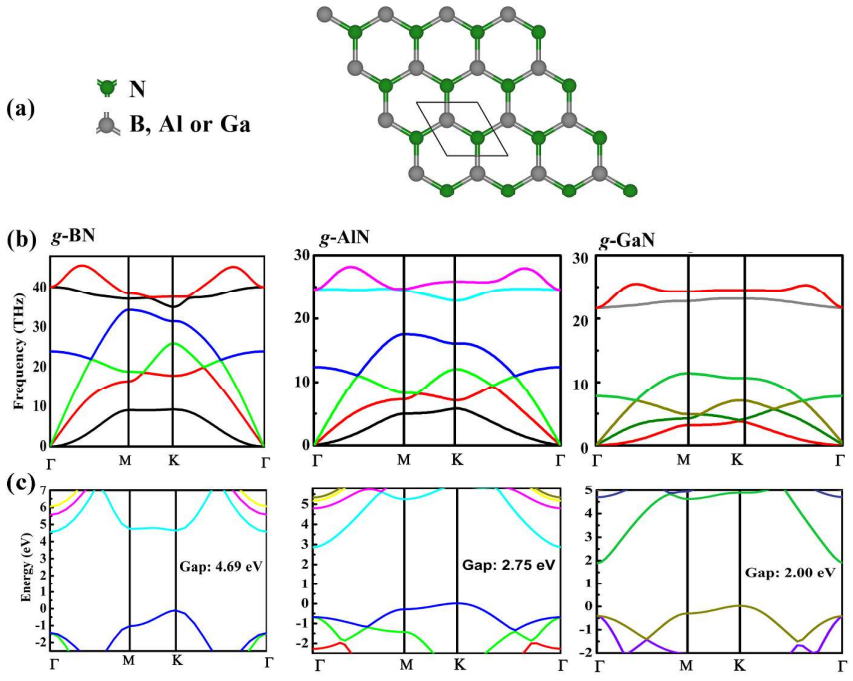


***Fig. 1*** *The (a) atomic structures, (b) phonon dispersions and (c) electronic band structures of g-XN (X=B, Al and Ga), calculated with PBE functional. Green and gray balls represent N and X atoms, respectively.*

### 3.2 $MoS_2$-XN heterostructures

As shown in **Fig. 2(a)**, the bilayer heterostructures are constructed by stacking $MoS_2$ and *g*-XN monolayers, denoted as $MoS_2$-XN for simplicity in the following. The calculated lattice constant of $MoS_2$ monolayer is 3.18 Å. We used the unit cells for $MoS_2$-AlN and $MoS_2$-GaN and got the optimized lattice constants of 3.16 Å and 3.23 Å, respectively. Thus the lattice mismatch between $MoS_2$ and *g*-AlN/GaN is quite small, only 0.9% and 1.8% for X=Al and Ga. The lattice mismatch between the unit cell of BN and $MoS_2$ is around 20%. To minimize the lattice mismatch between the two stacking sheets, a supercell that contains 4×4 $MoS_2$ and 5×5 *g*-BN unit cells of monolayer was employed. The optimized lattice constant of $MoS_2$-BN is 12.67 Å, with $MoS_2$ lattice being 0.4% compressed and *g*-BN lattice being 1.0% stretched.

The ground state geometries of $MoS_2$-XN heterostructures are determined by the

weak vdW interactions between neighboring layers. The equilibrium interlayer distance, $d_{MoS_2/XN}$, is defined as the distance between the S atoms in $MoS_2$ layers and the neighboring XN planes. In addition, the interlayer adhesion energy is calculated by the definition: $E_{ad} = (E_{MoS_2} + E_{XN} - E_{MoS_2/XN})/S$, where $E_{MoS_2/XN}$, $E_{MoS_2}$ and $E_{XN}$ represent the total energies of optimized $MoS_2$-XN heterostructures, the pure $MoS_2$ and *g*-XN monolayer, respectively, and *S* is the interface area.

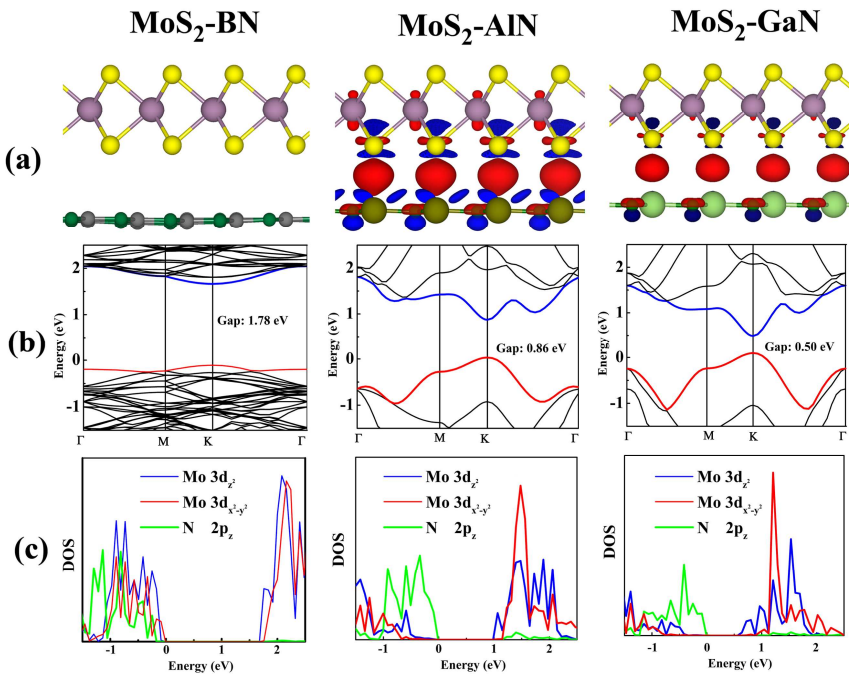


***Fig. 2*** *The (a) atomic structures, (b) band structures and (c) projected density of states (PDOS) of bilayer* $MoS_2$-XN *heterostructures, calculated with PBE functional. Purple, yellow, green, gray, dark-green, and pale-green balls represent Mo, S, N, B, Al, and Ga atoms, respectively. Charge accumulation (red) and depletion (blue) with respect to isolated* $MoS_2$ *and g-XN at the* $MoS_2$*/g-XN interface are also depicted in (a) and the isosurfaces is 0.008 e/Å*$^3$.

The calculated $d_{MoS_2/XN}$ for $MoS_2$-XN are 3.4 Å, 2.7 Å, and 2.9 Å for X = B, Al and Ga, respectively. The corresponding $E_{ad}$ for $MoS_2$-XN (X=B, Al and Ga) are 15 meV/Å$^2$, 26 meV/Å$^2$, and 20 meV/Å$^2$, respectively Both the interlayer distance and adhesion energy of $MoS_2$-XN are comparable with the values of bilayer $MoS_2$, i.e., $d_{bilayer\text{-}MoS_2}$ = 3.1 Å and $E_{ad}$ = 17 meV/Å$^2$. The smaller interlayer distance suggests the higher adhesion energy. So the $MoS_2$-AlN and $MoS_2$-GaN heterostructures should be

more stable than bilayer $MoS_2$.

To further understand the binding of the heterostructures, the three-dimensional charge density differences are calculated by subtracting the calculated electronic charge of $MoS_2$-XN from that of the independent $MoS_2$ and *g*-XN monolayers. As shown in **Fig. 2(a),** the charge transfer at the interface of $MoS_2$-BN is negligible, which agrees with the relatively large interfacial distance and small adhesion energy between $MoS_2$ and BN. Interestingly, charge densities of $MoS_2$-AlN and $MoS_2$-GaN exhibit large redistributions, especially at the interfacial region. The electron accumulation occurs at the interface and depletion is within the monolayers. Such a result suggests the $MoS_2$-AlN and $MoS_2$-GaN form the relatively strong adhesive interface.

The calculated band structures of the heterostructures are shown in **Fig. 2(b).** Interestingly, indirect band gaps of *g*-XN monolayers transform to direct ones in all $MoS_2$-XN heterostructures. For solar energy conversion applications, light with a photon energy close the band gap can produce an electron-hole pair. This process occurs quite easily in a direct band gap semiconductor because the electron does not need a large momentum. From this aspect, the direct-band-gap $MoS_2$-XN heterostructures are expected to have high solar energy conversion efficiency, compared to indirect-band-gap *g*-XN monolayers.

The calculated band gaps change among 0.50~1.78 eV for heterostructures with PBE functional. It has been well recognized that the typical DFT with GGA level is inadequate to describe the electronic structures of some semiconductors and usually underestimates the band gap due to the spurious electronic self-interaction present within this theory. The Heyd-Scuseria-Ernzerhof (HSE06) hybrid functional can usually predict more reasonable band gaps than GGA. For example, the band gap of monolayer *g*-BN monolayer is 4.69 eV with GGA calculation, but is 5.69 eV with HSE06 calculation, much closer to the experimental value (~6.07 eV[20]). Therefore the band gaps are further examined with the HSE06 functional. As shown in **Fig. S1**, HSE functional only enlarges band gaps compared with the PBE, but does not change the trend of electronic structures. More interestingly, both the heterostructures of $MoS_2$/GaN and $MoS_2$/AlN exhibit modest band gaps. For example, the band gap of $MoS_2$/AlN is about 2.00 eV, which is greatly favorable for the adsorption of the visible light.

As shown in **Fig. 2(c)**, the projected density of states (PDOS) clearly depict the valence band maximum (VBM) and the conduction band minimum (CBM) of heterostructures. In single-layer $MoS_2$, VBM and CBM are contributed by Mo-3$d_{x^2-y^2}$ and Mo-3$d_{z^2}$, while in single-layer *g*-XN, they are contributed by N-2$p_z$ and N-2$p_x$+$p_y$, respectively.[39] The detailed band alignments of $MoS_2$-XN heterostructures are shown in **Fig. 3(a)**, where the band edge positions are calculated with HSE06. The formation of type-II heterostructures is an effective approach to enhance charge separation efficiency for improved photocatalytic activity and water splitting efficiency. In a type-II band alignment, the position of VBM and CBM of a semiconductor, i.e. *g*-XN,

is higher than that of another, i.e. $MoS_2$. **Fig. 3(a)** indicates that $MoS_2$-AlN and $MoS_2$-GaN belong to type-II band alignments whereas $MoS_2$-BN does not. Thus the VBM and CBM of $MoS_2$-BN heterostructure preserve the same feature of $MoS_2$ monolayer, and both the VBM and CBM charges concentrate on the $MoS_2$ side for $MoS_2$-BN, as shown in **Fig. 3 (b)**. However, the VBM of $MoS_2$-AlN and $MoS_2$-GaN comes from N-2$p_z$. This indicates a complete separation of VBM and CBM on *g*-XN and $MoS_2$ monolayers, respectively, in $MoS_2$-AlN and $MoS_2$-GaN, as depicted more clearly in **Figs. 3 (c) and (d)**. It is well known that one of most effective ways to enhance photocatalytic activity is to avoid electronics-hole pair recombination[40, 41]. The photo-generated electronic and holes will be spontaneously separated for $MoS_2$-AlN and $MoS_2$-GaN heterostructures, which suppresses charge recombination and enhance the photocatalytic efficiency.

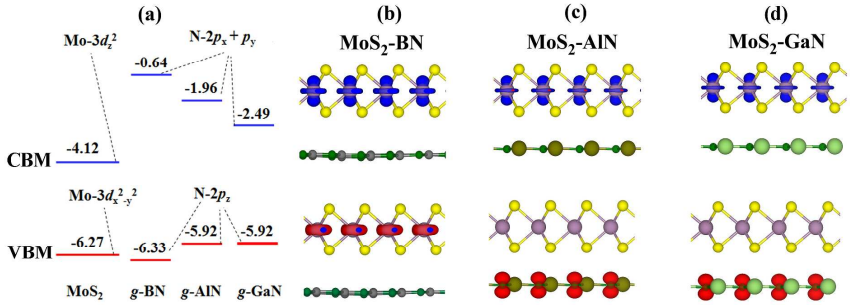


***Fig. 3*** *(a) Schematic energy band alignment between MoS2 and XN relative to the vacuum energy (The unit is eV). The corresponding charge densities of heterostructures are shown in (b) $MoS_2$/g-BN, (c) $MoS_2$/g-AlN and (d) $MoS_2$/g-GaN (an isosurface value of 0.04 e/Å$^3$). The VBMs are shown in red isosurfaces (lower panel), and CBMs in blue isosurfaces (upper panel). Purple, yellow, green, gray, dark-green, and pale-green balls represent Mo, S, N, B, Al, and Ga atoms, respectively.*

Besides bilayer heterostructures as discussed above, we also study the trilayer sandwiched heterostructures: one $MoS_2$ (*g*-XN) monolayer is sandwiched by two *g*-XN ($MoS_2$) monolayers, denoted as trilayer-I (-II). The calculated atomic configurations and band structures with the HSE06 functional of $MoS_2$-AlN and $MoS_2$-GaN trilayer heterostructures are shown in **Fig. 4**. The trilayer structure shows similar electronic structure profiles as bilayer heterostructure. For example, the direct band gap of trilayer-I $MoS_2$/AlN heterostructure is 1.90 eV, very close to the corresponding value of 2.00 eV in the bilayer structure. So both the bilayer and trilayer-I $MoS_2$/AlN heterostructures are favorable for the solar energy conversion. Nevertheless, we note that the trilayer-II heterostructure, which contains two $MoS_2$ monolayers, only has a smaller indirect band gap, exactly as the case of bilayer $MoS_2$ becoming indirect one (as shown in **Fig. S2**).

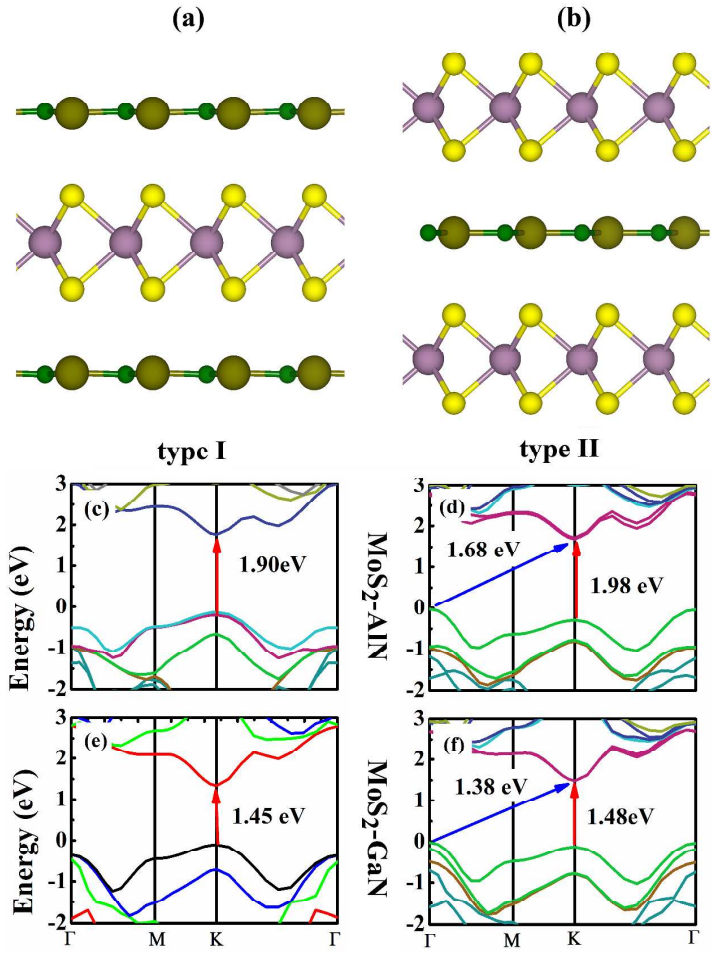


***Fig. 4*** *The (a)-(b) atomic configurations and (c)-(f) band structures of sandwiched trilayer type I (a) and type II (b) $MoS_2$-XN heterostructures, calculated with HSE06 functional. In trilayer I (type II) heterostructures, one $MoS_2$ (g-XN) monolayer is sandwiched by two g-XN ($MoS_2$) monolayers.*

### 3.3 Photocatalytic ability

The photocatalyst process in water splitting includes two reactions:

$2H_2O + 4h^+ \rightarrow O_2 + 4H^+$

$2H^+ + 2e^- \rightarrow H_2$

Therefore, in addition to an appropriate band gap of the semiconductor, a good photocatalyst material generally needs suitable VBM and CBM energy levels: a VBM energy lower than the oxidation potential (-5.67 eV) of $H_2O/O_2$ to first splitting water, and a CBM energy higher than the reduction potential (-4.44 eV) of $H^+/H_2$ to further producing $H_2$. The CBM and VBM energy levels for all materials calculated with HSE06 with respect to the vacuum energy level are shown in **Fig. 5**. Except the trilayer II $MoS_2$-AlN and $MoS_2$-GaN, the VBM positions of other materials vary from

-5.97 eV to -5.92 eV, which are obviously lower than the oxidation potential. On the other hand, the CBM energy of $MoS_2$-GaN bilayer and trilayer I structures are a little lower than the reduction potential. **Fig. 5** clearly depicts that the $MoS_2$-AlN bilayer and trilayer I heterostructures are suitable for solar energy conversion applications among these 2D materials.

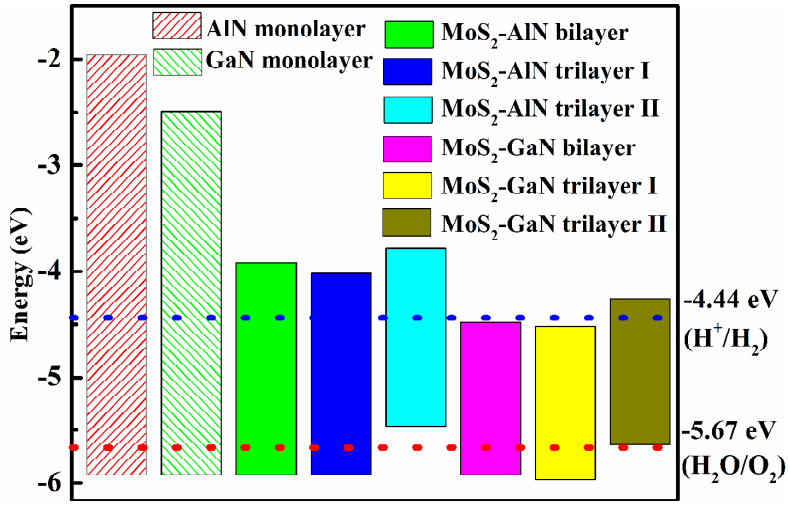


***Fig. 5*** *The band alignments of 2D materials from HSE06.*

In order to fully utilize the solar energy, another vital requirement for a high-performance photocatalytic material is that it should have a wide adsorption range of solar energy. The optical absorption coefficients directly reflect the absorption range of the spectrum and are critical in solar energy conversion realm. The optical adsorption spectrum of bilayer heterostructures are obtained by calculating the imaginary part of the complex dielectric function[42] with HSE06. The solar energy is mainly distributed in visible (50%) and infrared light (43%). However, traditional photocatalysts such as $TiO_2$ are mostly active only under ultraviolet irradiation.[43, 44] **Fig. 6** shows that the present heterostructures possess a relatively stronger adsorption index in visible light range (390-760 nm, 1.64-3.19 eV) than $MoS_2$. In particular, although the $MoS_2$ dos not have obvious adsorption index in the infrared light (<1.64 eV), $MoS_2$-GaN heterostructure exhibits considerable adsorption index in infrared light zone. Such results indicate that the efficiency of solar energy utilization of $MoS_2$ could be largely improved by heterostructures with AlN and GaN.

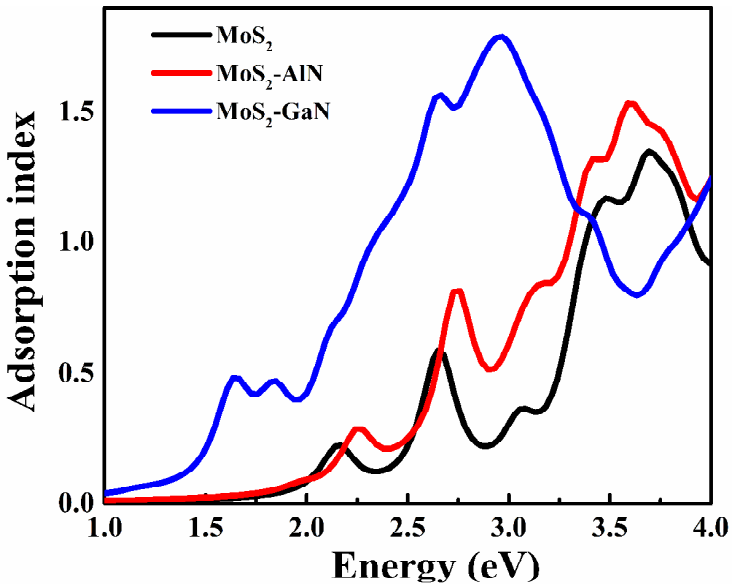


***Fig. 6*** *Calculated optical absorption spectra of $MoS_2$ and the bilayer heterostructures by using HSE06 functional.*

## 4. Conclusions

In summary, the phase stability and electronic properties of graphene-like 2D *g*-XN (X=B, Al, and Ga) monolayers and heterostructures with $MoS_2$ are carefully investigated through self-consistent vdW-DF calculations. We found that the *g*-AlN and *g*-GaN monolayers have thermodynamic stabilities exactly as *g*-BN through phonon calculations, exploring new graphene-like 2D structures that might be synthesized experimentally. The indirect band gaps in *g*-XN monolayers become direct gaps when stacking *g*-XN on a $MoS_2$ monolayer. In particular for X = Al and Ga, the $MoS_2$-AlN and $MoS_2$-GaN heterostructures show suitable band gaps (2.00 eV and 1.44 eV, respectively), complete electron-hole separation and strong optical adsorption index, making them promising candidates for solar energy conversion. Furthermore, $MoS_2$-AlN one is expected to be a good photocatalyst due to its suitable VBM and CBM alignments with the oxidation and reduction potentials of hydrogen generation from water. Our extensive investigations give insights for the development of novel 2D structures, with high performance for applications.

## Acknowledgments

This work was supported by the National Natural Science Foundation of China (No. 51222212), the CAEP foundation (Grant No. 2012B0302052), the MOST of China (973 Project, Grant NO. 2011CB922200). The computations supports from Informalization Construction Project of Chinese Academy of Sciences during the 11th Five-Year Plan Period (No.INFO-115-B01) are also highly acknowledged.

## References

1 K. S. Novoselov, A. K. Geim, S. V. Morozov, D. Jiang, Y. Zhang, S. V. Dubonos, I. V. Grigorieva, and A. A. Firsov, *Science*, 2004, **306,** 666.
2 W.-J. Yin, Y.-E. Xie, L.-M. Liu, R.-Z. Wang, X.-L. Wei, L. Lau, J.-X. Zhong, and Y.-P. Chen, *J. Mater. Chem. A*, 2013, **1,** 5341.
3 X. G. Luo, L.-M. Liu, Z. P. Hu, W.-H. Wang, W.-X. Song, F. F. Li, S.-J. Zhao, H. Liu, H.-T. Wang, and Y. J. Tian, *J. Phys. Chem. Lett.*, 2012, **3,** 3373.
4 X. Huang, Z. Zeng, S. Bao, M. Wang, X. Qi, Z. Fan, and H. Zhang, *Nature Commun.*, 2013, **4,** 1444.
5 M.-Q. Long, L. Tang, D. Wang, L. J. Wang, and Z. G. Shuai, *J. Am. Chem. Soc.*, 2009, **131,** 17728.
6 Y. F. Li, F. Y. Li, and Z. F. Chen, *J. Am. Chem. Soc.*, 2012, **134,** 11269.
7 Y. C. Wang, M. S. Miao, J. Lv, L. Zhu, K. T. Yin, H. Y. Liu, and Y. M. Ma, *J. Chem. Phys.*, 2012, **137,** 224108.
8 J. N. Coleman, M. Lotya, A. O'Neill, S. D. Bergin, P. J. King, U. Khan, K. Young, A. Gaucher, S. De, R. J. Smith, I. V. Shvets, S. K. Arora, G. Stanton, H. Y. Kim, K. Lee, G. T. Kim, G. S. Duesberg, T. Hallam, J. J. Boland, J. J. Wang, J. F. Donegan, J. C. Grunlan, G. Moriarty, A. Shmeliov, R. J. Nicholls, J. M. Perkins, E. M. Grieveson, K. Theuwissen, D. W. McComb, P. D. Nellist, and V. Nicolosi, *Science*, 2011, **331,** 568.
9 H. Zhang, L.-M. Liu, and W.-M. Lau, *J. Mater. Chem. A*, 2013, **1,** 10821.
10 J. F. Gao, J. J. Zhao, and F. Ding, *J. Am. Chem. Soc.*, 2012, **134,** 6204.
11 Y. D. Ma, Y. Dai, M. Guo, C. W. Niu, Y. T. Zhu, and B. B. Huang, *ACS Nano*, 2012, **6,** 1695.
12 T. Watanabe, J. Ohta, T. Kondo, M. Ohashi, K. Ueno, A. Kobayashi, and H. Fujioka, *Appl. Phys. Lett.*, 2014, **104,** 182111.
13 Y. Sun, Z. Sun, S. Gao, H. Cheng, Q. Liu, J. Piao, T. Yao, C. Wu, S. Hu, S. Wei, and Y. Xie, *Nature Commun.*, 2012, **3,** 1057.
14 A. K. Geim, and I. V. Grigorieva, *Nature*, 2013, **499,** 419.
15 L. Britnell, R. V. Gorbachev, R. Jalil, B. D. Belle, F. Schedin, A. Mishchenko, T. Georgiou, M. I. Katsnelson, L. Eaves, S. V. Morozov, N. M. R. Peres, J. Leist, A. K. Geim, K. S. Novoselov, and L. A. Ponomarenko, *Science*, 2012, **335,** 947.
16 A. Du, S. Sanvito, Z. Li, D. Wang, Y. Jiao, T. Liao, Q. Sun, Y. H. Ng, Z. Zhu, R. Amal, and S. C. Smith, *J. Am. Chem. Soc.*, 2012, **134,** 4393.
17 X. D. Li, S. Yu, S. Wu, Y.-H. Wen, S. Zhou, and Z.-Z. Zhu, *J. Phys. Chem. C*, 2013, **117,** 15347.
18 W. Zhou, Z. Yin, Y. Du, X. Huang, Z. Zeng, Z. Fan, H. Liu, J. Wang, and H. Zhang, *Small*, 2013, **9,** 140.
19 W. J. Yu, Z. Li, H. Zhou, Y. Chen, Y. Wang, Y. Huang, and X. Duan, *Nature Mater.*, 2013, **12,** 246.
20 L. Song, L. J. Ci, H. Lu, P. B. Sorokin, C. H. Jin, J. Ni, A. G. Kvashnin, D. G. Kvashnin, J. Lou, B. I. Yakobson, and P. M. Ajayan, *Nano Lett.*, 2010, **10,** 3209.
21 K. K. Kim, A. Hsu, X. Jia, S. M. Kim, Y. Shi, M. Hofmann, D. Nezich, J. F. Rodriguez-Nieva, M. Dresselhaus, T. Palacios, and J. Kong, *Nano Lett.*, 2011, **12,** 161.

22 X. X. Li, J. Zhao, and J. L. Yang, *Sci. Rep.*, 2013, **3,** 1858.
23 W. F. Li, M. Guo, G. Zhang, and Y.-W. Zhang, *Phys. Rev. B*, 2014, **89,** 205402.
24 W. Chen, E. J. G. Santos, W. Zhu, E. Kaxiras, and Z. Zhang, *Nano Lett.*, 2013, **13,** 509.
25 K. F. Mak, C. Lee, J. Hone, J. Shan, and T. F. Heinz, *Phys. Rev. Lett.*, 2010, **105,** 136805.
26 S. Cahangirov, C. Ataca, M. Topsakal, H. Sahin, and S. Ciraci, *Phys. Rev. Lett.*, 2012, **108,** 126103.
27 Y. F. Chen, J. Y. Xi, D. O. Dumcenco, Z. Liu, K. Suenaga, D. Wang, Z. G. Shuai, Y.-S. Huang, and L. M. Xie, *ACS Nano*, 2013, **7,** 4610.
28 B. Radisavljevic, A. Radenovic, J. Brivio, V. Giacometti, and A. Kis, *Nat Nano*, 2011, **6,** 147.
29 G. Kresse, and J. Furthmüller, *Phys. Rev. B*, 1996, **54,** 11169.
30 G. Kresse, and J. Furthmüller, *Comp. Mater. Sci.*, 1996, **6,** 15.
31 G. Kresse, and D. Joubert, *Phys. Rev. B*, 1999, **59,** 1758.
32 J. P. Perdew, K. Burke, and M. Ernzerhof, *Phys. Rev. Lett.*, 1996, **77,** 3865.
33 X. Wu, M. C. Vargas, S. Nayak, V. Lotrich, and G. Scoles, *J. Chem. Phys.*, 2001, **115,** 8748.
34 H. J. Monkhorst, and J. D. Pack, *Phys. Rev. B*, 1976, **13,** 5188.
35 A. Togo, F. Oba, and I. Tanaka, *Phys. Rev. B*, 2008, **78,** 134106.
36 K. Parlinski, Z. Q. Li, and Y. Kawazoe, *Phys. Rev. Lett.*, 1997, **78,** 4063.
37 Q. Li, D. Zhou, W. T. Zheng, Y. M. Ma, and C. F. Chen, *Phys. Rev. Lett.*, 2013, **110,** 136403.
38 B. Huang, and H. Lee, *Phys. Rev. B*, 2012, **86,** 245406.
39 X.-L. Wei, H. Zhang, G.-C. Guo, X.-b. Li, W.-M. Lau, and L.-M. Liu, *J. Mater. Chem. A*, 2014, **2,** 2101.
40 Y. Zhang, T. Mori, J. Ye, and M. Antonietti, *J. Am. Chem. Soc.*, 2010, **132,** 6294.
41 Y.-F. Li, and Z.-P. Liu, *J. Am. Chem. Soc.*, 2011, **133,** 15743.
42 R. M. Sheetz, I. Ponomareva, E. Richter, A. N. Andriotis, and M. Menon, *Phys. Rev. B*, 2009, **80,** 195314.
43 G. Liu, L.-C. Yin, J. Q. Wang, P. Niu, C. Zhen, Y. P. Xie, and H.-M. Cheng, *Energy Environ. Sci.*, 2012, **5,** 9603.
44 C. H. Sun, and D. J. Searles, *J. Phys. Chem. C*, 2013, **117,** 26454.